Research Article

Nano Biomed Eng

Application of Liposome Encapsulation Drug in Inhibiting Ferroptosis and Reducing Radiation Damage During Radiotherapy

Yongkang Zhou[1,§], Xuan Ding[2,§], Genwu Guo[1,§], Yuan Zhuang[1], Yixing Chen[1], Fuquan Zhang[1], Jian He[1]✉, Yunan Gao[1]✉

[1] Department of Radiation Oncology, Zhongshan Hospital, Fudan University, Shanghai 200032, China
[2] Department of Oncology, The First Affiliated Hospital of Chongqing Medical University, Chongqing 400016, China

[§]These authors contributed equally to this work.

✉ Corresponding author. E-mail: he.jian@zs-hospital.sh.cn; gao.yunan@zs-hospital.sh.cn

Received: Mar. 18, 2025; **Revised:** Mar. 25, 2025; **Accepted:** Mar. 28, 2025
Citation: Y.K. Zhou, X. Ding, G.W. Guo, et al. Application of liposome encapsulation drug in inhibiting ferroptosis and reducing radiation damage during radiotherapy. *Nano Biomedicine and Engineering*, 2025, 17(4): 517–528.
https://doi.org/10.26599/NBE.2025.9290124

Abstract

To alleviate the side effects of radiotherapy, amifostine, as the first FDA-approved radiation protectant, can be used to eliminate free radicals and regulate redox reactions. However, its application is limited by toxic side effects. Liposomes, as drug carriers, can efficiently encapsulate drugs and increase their concentration in tumor sites through passive targeting, reducing damage to normal tissues. Liposomes encapsulating antioxidant drugs can significantly inhibit ferroptosis caused by radiotherapy and alleviate lung and intestinal damage. Therefore, we prepared a novel nanomedicine with less toxic and highly effective radiation protectants based on liposome-encapsulated amifostine. By precisely regulating the ferroptosis pathway, it shows good radiation protection effects, providing a new strategy for the treatment of radiation pneumonitis and intestinal injury, and is expected to improve the quality of life and treatment outcomes of patients.

Keywords: amifostine; liposome; radiation damage; ferroptosis

Introduction

Radiotherapy (RT) holds a central position in cancer treatment and is an indispensable part of many tumor treatment plans [1]. This method directly attacks the DNA of cancer cells with high-energy radiation, effectively inhibiting their proliferation and division [2, 3], aiming to reduce tumor volume or completely eliminate cancer cells. Its application is not limited to direct treatment but also includes shrinking tumors before surgery to facilitate the operation or eliminating residual cancer cells after surgery to reduce the risk of recurrence [4]. Although RT demonstrates powerful therapeutic effects [5], it poses a potential threat to the surrounding normal tissues [6, 7], easily causing side effects such as radiation-induced pulmonary fibrosis and radiation enteritis [8], which significantly affect the quality of life and psychological state of patients. One of the roots of radiation-induced pulmonary fibrosis and radiation enteritis lies in radiation-induced ferroptosis [9, 10], an emerging form of cell death characterized by excessive accumulation of

free iron and activation of lipid peroxidation reactions within cells [11]. During RT, the radiation not only targets cancer cells but also damages sensitive tissues such as the lungs and intestines [12], activating the ferroptosis pathway, leading to loss of cell function, increased inflammatory responses, and tissue fibrosis. In this process, the imbalance of antioxidant defense mechanisms [13], especially the decline in glutathione and selenoenzyme levels [14], exacerbates the damage caused by oxidative stress to cells [15].

To alleviate the side effects of RT, scientists have developed various protective strategies. Amifostine (Ami), as the first radiation protectant approved by the US FDA [16], effectively inhibits radiation-induced ferroptosis by scavenging free radicals and regulating redox reactions, thereby protecting normal tissues [17]. However, its application is limited by dose-dependent toxic side effects such as hypotension and nausea [18]. To address this challenge, the innovative application of liposomes as drug carriers offers new opportunities for RT protection [19, 20]. Liposomes can efficiently encapsulate drugs, increasing these drugs' or their concentration in tumor sites through passive targeting mechanisms while reducing potential damage to normal tissues [21]. Studies have shown that encapsulating antioxidant drugs in liposomes can significantly inhibit RT-induced ferroptosis, thereby reducing damage to the lungs and intestines.

We have developed a low-toxicity and highly effective radiation protectant based on liposomes, aiming to achieve effective protection during RT by precisely regulating the ferroptosis pathway. Through *in vitro* and *in vivo* experiments, this protectant has demonstrated excellent radiation protection effects, providing a new strategy for treating radiation-induced pneumonia and intestinal damage, and offering patients a safer and more effective treatment option, which is expected to further improve their quality of life and treatment outcomes (Fig. 1).

Materials and Methods

Materials

1,2-Dipalmitoyl-sn-glycero-3-phosphatidylcholine (DPPC), 1,2-distearoyl-sn-glycero-3-phosphoethanolamine-*N*-(polyethylene glycol)-5000 (DSPE-PEG$_{5000}$), and cholesterol were purchased from Xi'an Ruixi Biological Technology Co., Ltd (China). DMEM medium, fetal bovine serum, penicillin-streptomycin (100×), trypsin-EDTA (0.25%), and phosphate-buffered saline (PBS) were provided by YEASEN Co., Ltd (China). The MTT assay kit and Ami were obtained from Meilun Biological Technology Co., Ltd (China). Anti-γ-H2AX antibody, bovine serum albumin (BSA), triton X-100, and anti-GPX4 antibody were purchased from Sigma-Aldrich (USA). Chloroform and cyanine5.5 (Cy5.5) fluorescent dye were acquired from Aladdin (China). The HRP-conjugated secondary antibody was obtained from Boster (China). Hematoxylin and eosin (H&E) staining kits were provided by MINDEL and Solarbio (China), while the DAB substrate kit and sodium citrate buffer were supplied by Solarbio (China). PrimeScript™ RT Master Mix and 2× EasyTaq® PCR SuperMix

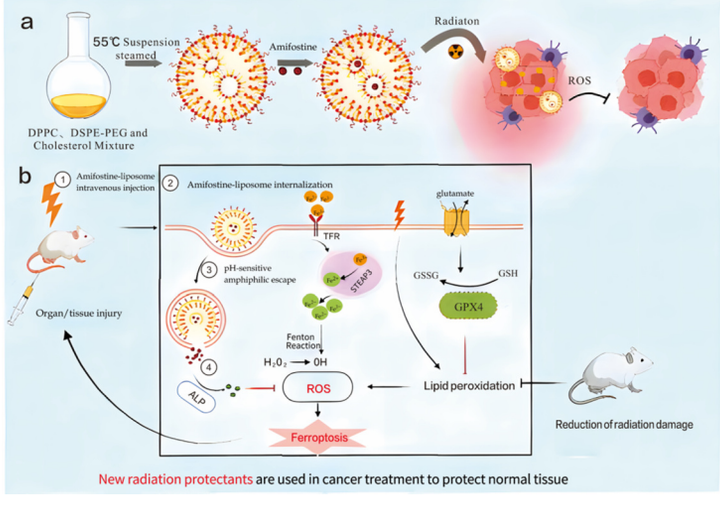

Fig. 1 Mechanism of liposome-encapsulated amifostine in inhibiting ferroptosis and reducing radiation damage. **(a)** Synthesis of amifostine-loaded liposomes and their inhibition of ROS production; **(b)** Amifostine lipsomes regulation of GPX4 inhibits ferroptosis and reduces radiation damage.

were sourced from Takara (Japan). RIPA lysis buffer and prestained protein molecular weight marker (10–180 kDa) were provided by Biosharp (China). The BCA protein assay kit was obtained from Beyotime (China), and RNA Later was supplied by Vazyme (China). Glutaraldehyde (for TEM) was sourced from Yuanye (China). Anti-GPX4 antibodies were provided by both Sigma-Aldrich (USA) and Affinity (China).

Preparation and characterization analysis of amifostine liposomes

Dipalmitoyl phosphatidylcholine (DPPC), DSPE-PEG_{5000}, and cholesterol were mixed in a molar ratio of 3:2:1 in a dried round-bottom flask. Amifostine (Ami) dissolved in chloroform was added to the mixture. The mixture was sonicated for 5 min to ensure homogeneity. The solvent was evaporated using a rotary evaporator at 55 °C until a thin lipid film formed. The lipid film was hydrated with 2 mL of dd H_2O, sonicated for 15 min, and stirred at 45 °C for 120 min. The suspension was extruded through polycarbonate membranes (400 and 200 nm) using a mini-extruder. The resulting liposomes were centrifuged at 10,000 r/min for 30 min. The pellet containing Ami liposomes (Pami) was collected. Particle size and distribution were measured using a DLS instrument. Crystallinity was analyzed via XRD. Chemical structure was confirmed using FTIR. Morphology and size were observed using a Talos 200X TEM.

Biocompatibility

Cells (5 000/well) were treated with Ami liposomes (0–200 μg/mL) for 24 h. MTT solution (10 μL) was added, incubated for 4 h, and absorbance at 570 nm was measured. BEAS-2B cells (900 cells/well) were pretreated with Ami liposomes (200 μg/mL) for 30 min, irradiated (0–6 Gy), and cultured for 14 days. Colonies were fixed with 4% paraformaldehyde and stained with crystal violet.

Flow cytometric analysis of ROS

After BEAS-2B cells were treated with drugs and exposed to radiation for 24 h, the culture medium was discarded, and the cells were washed with PBS. The cells were collected by centrifugation at 1 000 r/min for 5 min and then washed twice with PBS. A standard working solution was prepared by diluting the fluorescent probe in PBS at a ratio of 1:1 000 (cell suspension at 1×10^6 cells/mL). The cells were incubated with the probe solution at 37 °C in the dark for 1 h. Subsequently, the probe solution was removed by centrifugation, and the cells were washed twice with PBS. Finally, the cells were collected for fluorescence quantification analysis.

Fluorescent imaging

Cells were fixed with 4% paraformaldehyde and permeabilized with 0.5% Triton X-100 for 10 min at room temperature. Immunostaining was performed using rabbit anti-γ-H_2AX antibody at 4°C overnight. For the visualization of IR-induced foci, cells were irradiated with 2, 4, 6, and 8 Gy X-ray prior to immunostaining with fluorescein isothiocyanate-goat anti-rabbit IgG (H+L). Cell nuclei were stained with 4′,6-diamidino-2-phenyl-indole DAPI.

Spleen/thymus index in mice

BALB/c mice were euthanized using cervical dislocation. The abdominal cavity was then surgically opened, and the spleen and thymus were carefully dissected and removed to ensure their integrity. After harvesting, the organs were gently blotted on filter paper to remove any residual blood or fluid. The spleen and thymus were weighed with a high-precision electronic balance (e.g., Sartorius, ± 0.1 mg accuracy). Additionally, the body weight of each mouse was recorded in grams (g) right before euthanasia. The spleen index and thymus index were calculated as the ratio of the organ weight (mg) to the body weight (g).

IVIS spectrum imaging *in vivo*

Cy5.5 was covalently conjugated with Ami-loaded liposomes through constant-rate stirring at room temperature. The labeled liposomes were purified via dialysis and ultrafiltration to prepare the fluorescent probes. Four female BALB/c mice were intravenously injected with Cy5.5-labeled liposomes via the tail vein. Major organs (heart, liver, spleen, lungs, kidneys) were harvested at 2, 4, 12, and 24 h time points post-injection. The excised tissues were rinsed with normal saline, arranged on a black imaging plate according to anatomical order, and subjected to fluorescence signal acquisition using an IVIS Spectrum imaging system.

Animal behavior assessment

Initial body weights were recorded and mice were numbered prior to the experiment. The corresponding drug treatments (Ami or Ami liposomes) were administered 30 min before 4 Gy total body irradiation (TBI). Post-irradiation monitoring was conducted for 30 consecutive days, with daily measurements of body weight changes and quantitative evaluation of motor function using a standardized behavioral assessment scale.

Western blot

Tissue lysates were prepared with RIPA buffer, and protein concentrations were quantified by BCA assay.

Equal amounts of protein were separated by SDS-PAGE, transferred to PVDF membranes, and blocked with 5% skim milk. Membranes were incubated with primary antibodies (anti-[Target Protein], 1:1 000) and HRP-conjugated secondary antibodies (1:5 000), followed by ECL detection.

RNA extraction and quantitative real-time PCR

Take 80 mg of the tissue sample, add 1 mL of Trizol and steel beads, shake to break up and then vortex to mix well, and let it stand for 5 min. Add 200 μl of chloroform, shake and let it stand to stratify, then centrifuge at 4 °C and 12 000 r/min for 10 min. Transfer the upper aqueous phase to a new tube, add an equal volume of isopropanol to precipitate RNA, let it stand at room temperature for 8 min and then centrifuge again (as before), then discard the supernatant. Wash the precipitate twice with 75% ethanol, centrifuge to remove the residual ethanol, dry at room temperature, and dissolve in 50 μL of DEPC water. The concentration and purity of RNA are determined by NanoDrop. Use the PrimeScript™ RT Master Mix kit. The reaction system consists of 4 μL of Master Mix, 1 μg of RNA template, and RNase-free water to a total volume of 20 μL. The reaction program is as follows: 37 °C for 15 min (reverse transcription), 85 °C for 5 seconds (enzyme inactivation), and 10 °C to terminate the reaction, obtaining cDNA. Use the SYBR Green method. The reaction system includes 5 μL of 2× SYBR qPCR SuperMix, 2 μL of cDNA, 0.5 μL of forward and reverse primers (final concentration 0.2 μmol/L), and 2 μL of RNase-free water, with a total volume of 10 μL. The qPCR program is as follows: initial denaturation (50 °C for 2 min, 95 °C for 15 s), 40 cycles of amplification (95 °C for 15 s, 60 °C for 1 min). Use β-actin as the internal reference gene, and calculate the relative expression level of the target gene (such as GPX4) using the $2^{-\Delta\Delta C_t}$ method. All steps use RNase-free consumables, and the operation is carried out in a laminar flow hood to prevent RNA degradation. The specificity of the primers is verified by melting curve analysis.

Immunohistochemistry

Paraffin-embedded sections were deparaffinized, rehydrated, and subjected to antigen retrieval. Endogenous peroxidase activity was blocked with 3% H_2O_2, and non-specific binding was inhibited with 5% BSA. Sections were incubated with primary antibodies (anti-[Target Protein], 1:200) overnight at 4 °C, followed by HRP-conjugated secondary antibodies (1:500). Protein localization was visualized using DAB substrate and counterstained with hematoxylin.

Statistical analysis

All data were expressed as mean ± SD/SEM. Student's *t*-test (two-tailed) or one-way analysis of variance was performed in this study. All statistical analyses were performed using GraphPad Prism 8.00 (GraphPad Software Inc., USA). The probability values less than 0.05 were considered statistically significant. The detailed statistical analysis description is given in each figure caption.

Results

Structure and characterization of Ami liposomes

The structure, synthesis process, and mechanism of action of Ami liposomes are shown in Fig. 2(a). The DLS particle size analysis results indicated that the particle size of Ami liposomes was approximately 150 nm, with a nearly normal distribution, which was within the particle size range of nanodrugs (Fig. 2(b)). Then, the XRD diffraction spectrum showed that Ami liposomes exhibited an amorphous structure (Fig. 2(c)). Subsequently, FTIR infrared spectroscopy revealed that the characteristic peaks of Ami liposomes overlapped with those of Ami and liposomes, indicating that the material properties changed after the synthesis of Ami and liposomes, while their chemical structures remained unchanged (Fig. 2(d)). Finally, from the transmission electron microscopy, it was observed that Ami was encapsulated within the phospholipid bilayer, forming a smooth spherical structure. The diameter obtained from the electron microscopy image was approximately 150 nm, which was consistent with the DLS particle size detection results (Fig. 2(e)).

In vitro radiation protection experiment

The results of the MTT experiment showed that the proliferation activity of GC-1 cells, BEAS-2B cells, and TEC cells was not significantly reduced when the concentration of Ami liposomes was as high as 0.2 mg/mL, indicating that Ami liposomes did not have proliferation toxicity to cells (Fig. 3(a)). The proliferative activity of each group of cells was measured by MTT assay, and the radiation protective effect of fostatin liposomes was evaluated (Fig. 3(b)). With the increase of irradiation dose, the cell viability showed

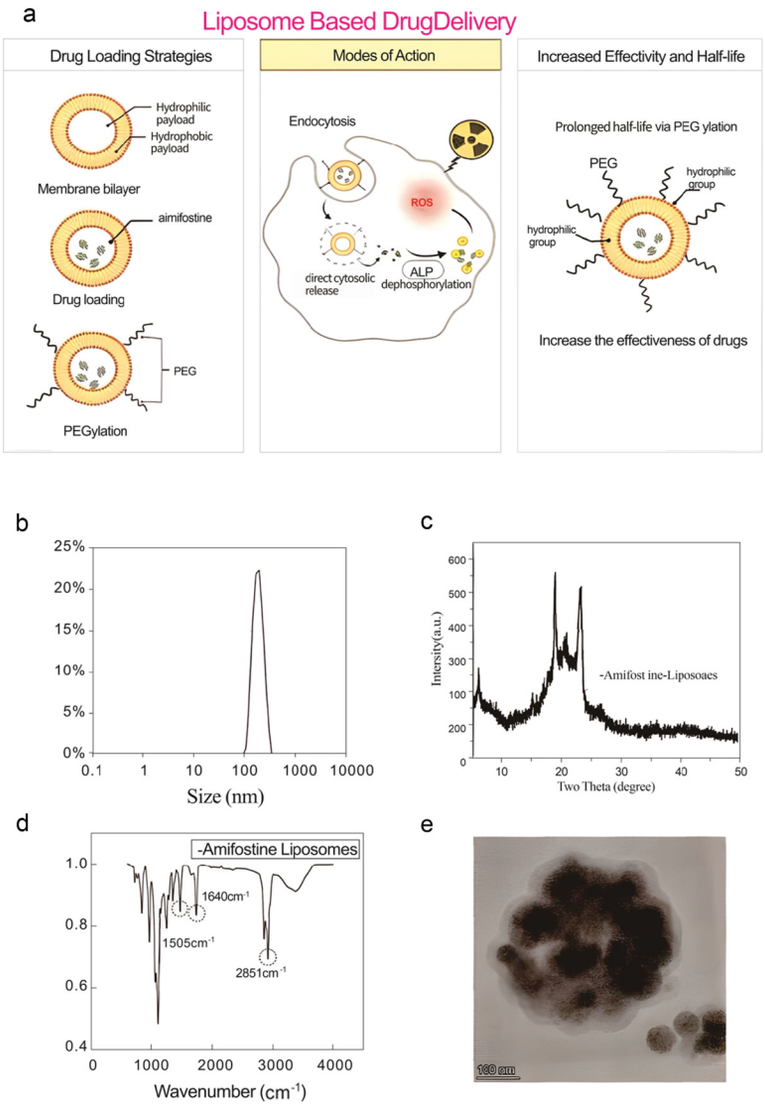

Fig. 2 Characterization of amifostine liposomes: **(a)** schematic diagram of the structure, synthesis process, and mechanism of action of amifostine liposomes; **(b)** DLS particle size distribution of amifostine liposomes; **(c)** XRD spectrum of amifostine liposomes; **(d)** FTIR spectrum of amifostine liposomes; **(e)** TEM image of amifostine liposomes.

a decreasing trend, and the cell proliferation activity was obviously limited when the cells were irradiated at 6 Gy. At this time, the cell viability of the Ami liposome group was much higher than that of the Ami group, indicating that the Ami liposome group had a better radiation protective effect than the Ami group. We further verified the *in vitro* radiation protective effect of Ami liposomes through clonal formation experiments. The RT+Pami group had the most significant protective effect when the irradiation dose was 4 Gy with the highest number of clones (Fig. 3(c)).

In order to explore whether Ami liposomes can achieve radiation protection by alleviating DNA damage and clearing ROS, we conducted DNA double-strand break marker γ-H2AX staining. The results showed that, compared with the CTL group, the DNA double-strand break appeared significantly in the RT group after 4 Gy irradiation. In contrast, DNA double-strand breaks in the RT+Pami group were significantly lighter, and the degree of DNA damage in this group was lower than that in the RT+Ami group (Fig. 3(d)), indicating that amifotine liposomes could effectively reduce the DNA damage caused by RT, thus achieving radiation protection. The intracellular ROS levels were detected (Fig. 3(e)), and the results showed that the ROS levels in the RT group were significantly higher than those in the CTL group, while the ROS levels in the RT+Pami group were significantly lower than those in the RT group. The above results indicated that ionizing radiation would cause DNA

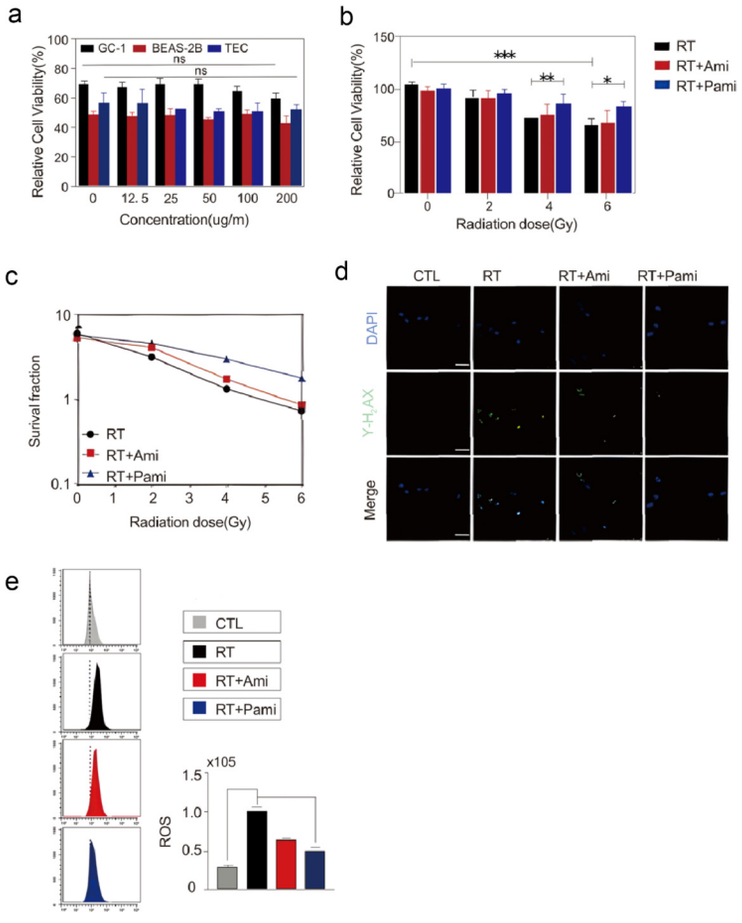

Fig. 3 Radiation protective effects of amifostine liposomes. **(a)** Relative cell survival rates of GC-1, BEAS-2B, and TEC cells incubated in amifostine liposomes with different concentrations for 24 h; **(b)** Cell viability assay of BEAS-2B treated with amifosine liposomes at different radiation doses of 0/2/4/6 Gy; * indicates the comparison between the RT group and the RT+Pami group; **(c)** Colony formation assay using the same treatment method as in (b) to determine the clonogenic survival rate of the cells; **(d)** Confocal images of gamma-H2AX-labeled double-stranded DNA breaks (blue: DAPI, green: gamma-H2ax, scale bar = 50 mm). The X-ray irradiation dose was 4 Gy. **(e)** Flow cytometry analysis of intracellular ROS in BEAS-2B. The results are expressed as means ± SEM: $*P < 0.05$, $**P < 0.01$, $***P < 0.001$.

double-strand breakage, and the production of ROS. Ami liposomes could achieve radiation protection by removing the ROS produced by irradiation and reducing DNA damage.

Metabolic distribution *in vivo*

Cy5.5-labeled Ami liposomes was shown in Fig. 4(a). In order to observe the distribution and metabolism of Ami liposomes in different time periods *in vivo* (Fig. 4(b)), Cy5.5-labeled Ami liposomes were injected into four mice through the tail vein (63.6 mg/kg for each mouse). The heart, liver, spleen, lung, and kidney at 4 time points (2, 4, 12, and 24 h) were collected, and the drug distribution at 24 h was tracked by an IVIS Spectrum animal living optical imager. The results showed that, based on time-dependent IVIS imaging data, the uptake of Ami liposomes in the liver reached the highest level 2 h after drug injection, and then gradually decreased and disappeared with the extension of time. The content of Ami liposomes in the kidney at 4 and 12 h was relatively the highest and began to decrease after 24 h. This indicated that Ami liposomes did not accumulate in the liver, remained in the body for about 24 h, and were metabolically cleared in the body mainly by the kidney (Fig. 4(c)). The above results show that Ami liposomes do not accumulate *in vivo*, have little toxicity and can be excreted from mice through metabolism, and do not cause short-term side effects to normal mice, and hence have the prospect of biomedical application *in vivo*.

Radiation damage under TBI

According to the calculation method of human and animal body surface area, the drug dose of mice was converted. It is known that the dosage of Ami used in

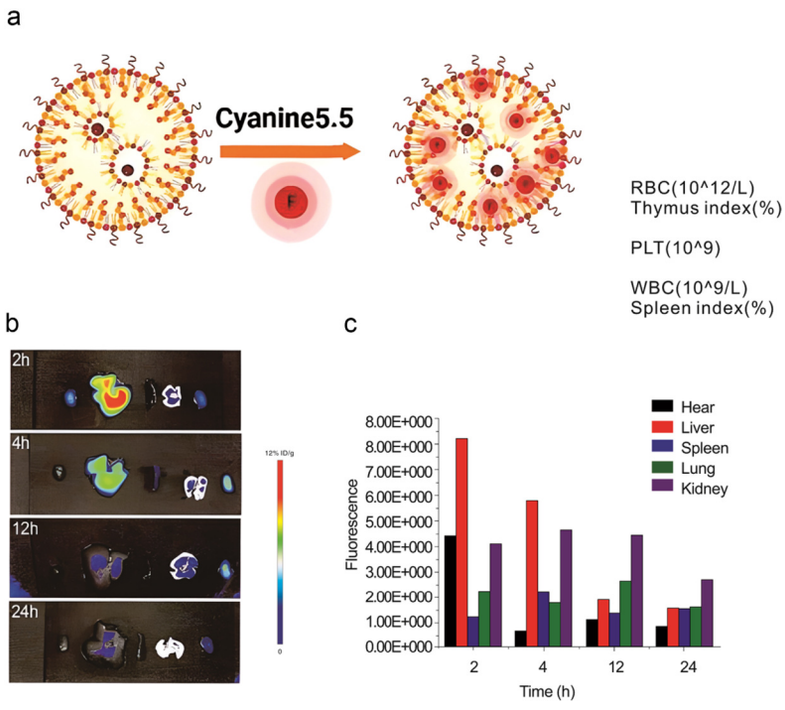

Fig. 4 Cy5.5-labeled amifostine liposomes' IVIS Spectrum *in vivo* imaging of small animals. **(a)** Schematic diagram of Cy5.5-labeled amifostine liposomes passing through a chelation-free mode; **(b)** Fluorescence distribution of labeled amifostine liposomes in the heart, liver, spleen, lung, and kidney at different time points; **(c)** Changes in the distribution of labeled amifostine liposomes in different organs over time.

clinical RT is 200–300 mg/m^2, and the calculated trial dose of mice is 63.6 mg/kg, which is administered through the tail vein 30 min before irradiation; the experimental groups are shown in Fig. 5(a). The 30-day weight change trend and 30-day behavioral score of mice were recorded after 24 h of irradiation. The statistical results showed that compared with mice in the CTL group, the weight of mice in the RT group decreased in the first 6 days and then increased. After the 20th day, the mice gradually healed themselves, and their weight returned to the original weight and gradually increased. After TBI, the weight of mice in the RT+Ami group and RT+Pami group decreased significantly in the first 5 days, and then began to increase and gradually exceeded the initial weight until the 30th day. Among them, the weight increase trend of the RT+Pami group was higher than that of the RT+Ami group (Fig. 5(b)), indicating that Ami liposomes could more effectively alleviate the weight loss of mice induced by ionizing radiation. The results of clinical behavioral scores showed that the RT group had the highest scores, indicating inflammatory infiltration and demyelination in the central nervous system tissues of mice after irradiation. On the contrary, the clinical behavioral scores of mice in the RT+Pami group were lower than those in the RT group, and the scores of mice in the RT+Pami group were close to those in the CTL group (Fig. 5(c)). These data indicate that Ami liposomes can inhibit weight loss and reduce central nervous system injury in irradiated mice at the irradiation dose of 4 Gy, indicating that Ami liposomes have a significant radiation protective effect *in vivo*.

The protective function of the hematopoietic system

Ami liposomes showed radiation protection in TBI experiments in mice. In order to further explore whether the protective effect of Ami liposomes is systemic or local, and whether it is universal or selective to organs and tissues, based on the above problems, we tested the indicators related to the hematopoietic system and liver injury. According to the results of spleen index and thymus index (Figs. 6(a) and 6(b)), compared with the CTL group, the spleen index and thymus index of mice in the RT group were decreased, while the spleen index and thymus index of mice in the RT+Pami group were higher than those in the RT group, indicating that injection of amifotine liposome could enhance the immunity and radiation resistance of mice. Blood biochemical results showed that the number of white blood cells, red blood cells, platelets, and hemoglobin were decreased in the RT group. Compared

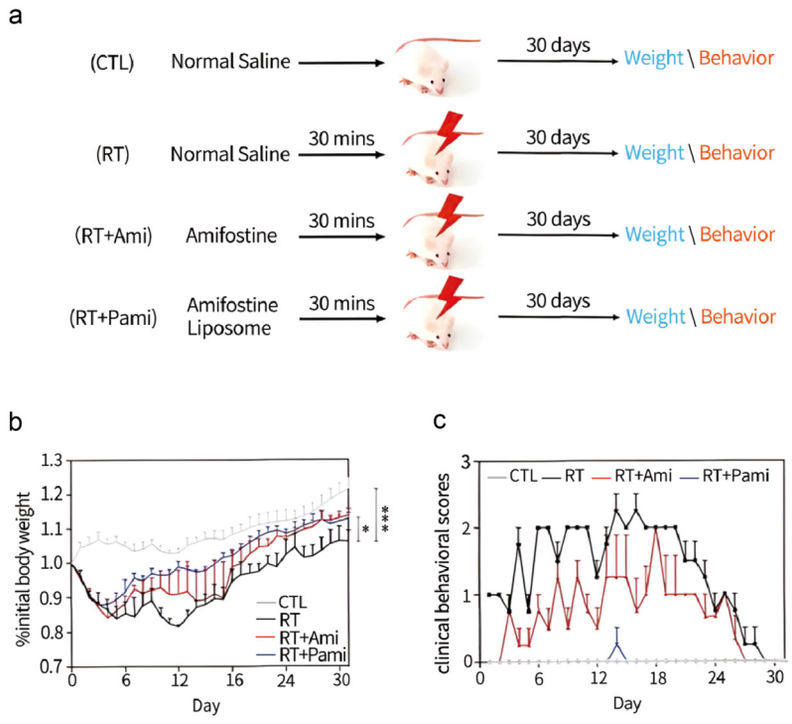

Fig. 5 The survival rate and behavioral score of mice with TBI improved by amifostine liposomes. **(a)** Schematic diagram of the experimental design; **(b)** 30-day weight change curve of TBI mice (n = 4/group); **(c)** 30-day behavioral score curve of TBI mice (n = 4/group). The results are expressed as means ± SEM. *P < 0.05, ***P < 0.001, and ****P < 0.001.

with the RT group, leukocyte, red blood cell, platelet, and hemoglobin counts were increased in the RT+Pami group (Figs. 6(c)–6(f)). Aspartate transaminase (AST) and alanine aminotransferase (ALT) indexes of liver injury were also detected (Figs. 6(g) and 6(h)). The contents of AST and ALT in the RT group were increased, indicating that the liver function of mice was impaired after irradiation. Compared with the RT group, AST and ALT contents in the RT+Pami group were significantly decreased, indicating that Ami liposomes could protect the liver from radiation damage. These results indicated that Ami liposomes had a protective effect on the hematopoietic system in TBI.

Reduce radiation-induced intestinal and pulmonary injuries

In order to further explore the protective effect of amifotine liposomes on tissues and organs, mice treated with different treatments were treated with 4 Gy TBI and euthanized 24 h later; the liver, spleen, thymus, colon, and lung tissues of mice were obtained, and tissue damage was evaluated with H&E staining (Figs. 7(a) and 7(b)). 24 h after TBI, the lung tissue of mice in the RT group showed obvious inflammatory cell infiltration, the height of colonic villi decreased, a large number of crypts appeared, and inflammatory cells around the glands increased. Amifotene liposomes improved pulmonary inflammation, decreased the relative height of intestinal villi, decreased the number of crypts, and other tissue damage was not obvious. The results showed that the lung tissue and colon tissue of mice after TBI were damaged to different degrees, while the radiation intestinal injury and lung injury of mice in the RT+Pami group were not obvious. The results of H&E staining showed that Ami liposomes could protect lung and colon tissues from radiation damage and had the potential to become anti-radiation protective drugs *in vivo*.

Ami liposomes inhibit ferroptosis

In order to verify that Ami liposomes regulate the expression level of GPX4 protein and inhibit ferroptosis after irradiation, we investigated the regulatory ability of Ami liposomes on GPX4 protein by Western blot and Q-PCR experiments. The results showed (Figs. 8(a) and 8(b)) that GPX4 protein and gene expression levels in the colon and lung tissues of irradiated mice were significantly decreased compared with those of the unirradiated group, while protein and gene expression levels of GPX4 were increased after injection of Ami liposomes into the tail vein and subsequent irradiation, which was consistent with our GPX4 immunohistochemical results. In addition, the morphological

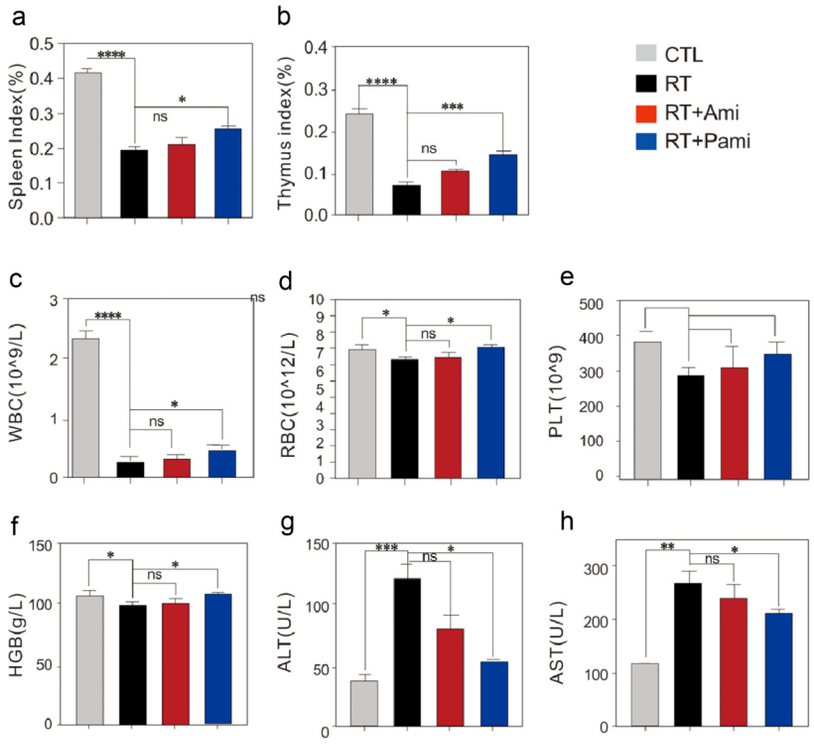

Fig. 6 Amifostine liposomes alleviated hematopoietic system and liver injury. **(a)** Spleen index = spleen/body weight (g); **(b)** Thymus index = thymus (g)/body weight (g); **(c)** Mouse WBC count; **(d)** RBC counts; **(e)** PLT count; **(f)** HGB count; **(g)** ALT concentration; **(h)** AST concentration. Results are expressed as means ± SEM. **P* < 0.05, ***P* < 0.01, ****P* < 0.001, *****P* < 0.0001 (*n* = 4/group).

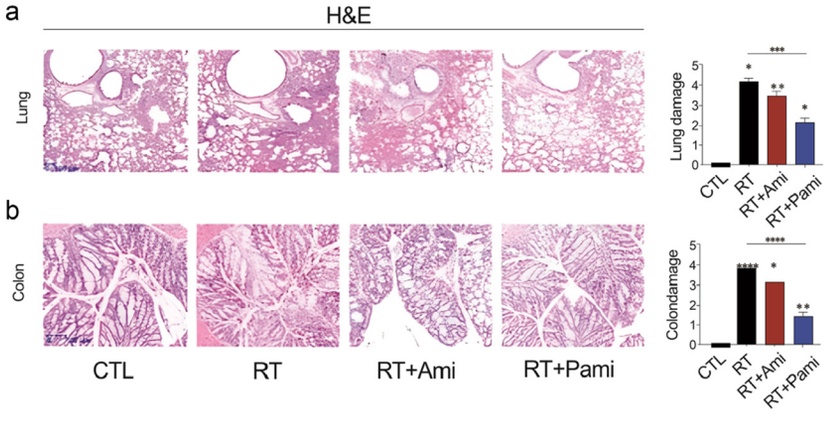

Fig. 7 Amifostine liposomes alleviated lung and colon injury (H&E staining). **(a)** H&E-stained images of lung tissue and pathological scores of tissue injury after different treatments of mice; scale bar = 100 μm. **(b)** H&E-stained images of colon tissue and pathological scores of tissue injury of mice after different treatments; scale bar = 100 μm.

structure of mitochondria was observed by transmission electron microscopy (Fig. 8(c)). The results showed that the surface of mitochondria in the RT group shrank, mitochondrial ridges decreased or even disappeared, and mitochondrial membrane density increased, which are the typical morphological characteristics of ferroptosis. These results indicated that ionizing radiation could cause ferroptosis in cells, and the morphology and structure of mitochondria were not significantly damaged after the addition of Ami liposomes, which was similar to that of normal mitochondria in the CTL group. These results indicate that Ami liposomes can protect mitochondria from the damage of ionizing radiation. The above data indicate that Ami liposomes can regulate the expression of GPX4 in cells, inhibit the pathway of ferroptosis in cells, alleviate the damage of ionizing radiation on mitochondria, and thus play a role in radiation protection.

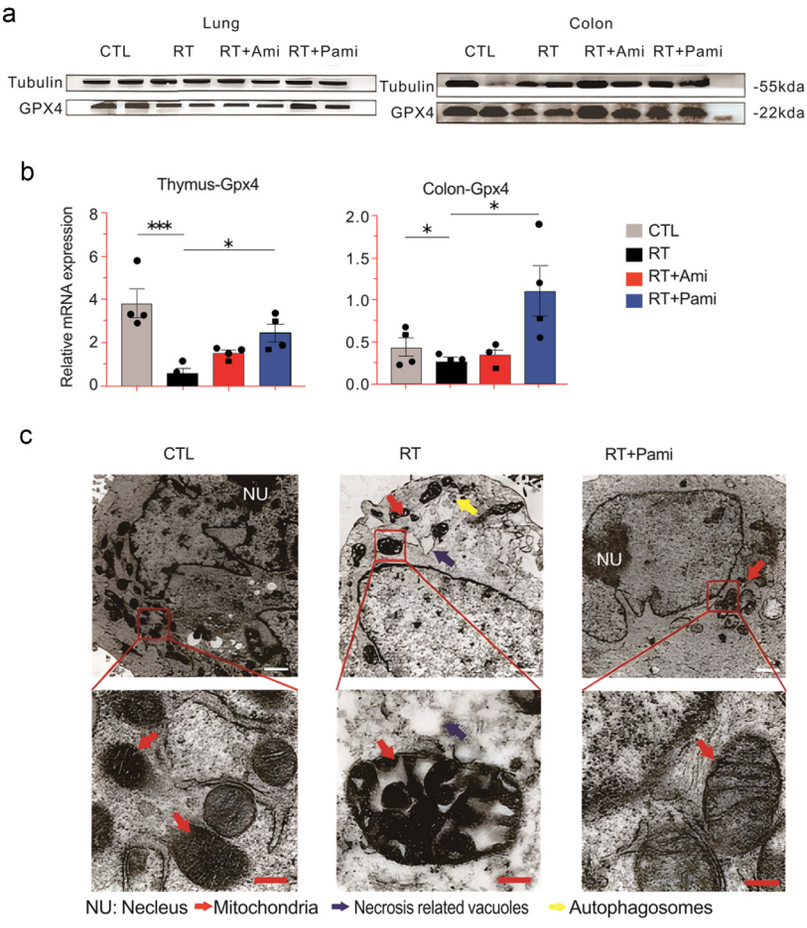

Fig. 8 Amifostine liposomes inhibited ferroptosis in irradiated cells. **(a)** GPX4 protein expression in the lung and colon of mice exposed to 4 Gy TBI for 24 h was analyzed by Western blot. **(b)** GPX4 gene expression in the lung and colon of mice was analyzed by Q-PCR. The results are expressed as means ± SEM; $^{*}P < 0.05$, $^{**}P < 0.01$, $^{***}P < 0.001$ ($n = 4$/group). **(c)** Transmission electron microscopy (TEM) images of BEAS2B cells 24 h after irradiation. Nu, nucleus; red arrow, mitochondria; yellow arrow, autophagosome; black arrow, necrosis-associated vacuoles. Scale bar: upper side, 5 μm; lower side, 500 nm.

Discussion

This study developed a novel nano-radioprotective agent by encapsulating Ami in liposomes and systematically elucidated its mechanism of action in mitigating radiation-induced lung and intestinal damage through the inhibition of ferroptosis. The experimental results demonstrated that the liposome-encapsulated technology significantly enhanced the bioavailability and targeting of Ami, while reducing its dose-dependent toxicity, providing an innovative strategy for optimizing existing radioprotective agents.

First, *in vitro* experiments confirmed that liposome-encapsulated Ami could effectively scavenge radiation-induced reactive oxygen species (ROS), reduce DNA double-strand breaks (γ-H2AX foci), and significantly increase cell survival rates (Fig. 3). Compared with free Ami, the liposome group showed stronger radioprotective effects at the same dose, which might be attributed to the passive targeting characteristics of liposomes that prolonged the drug's retention time in the tumor microenvironment and reduced non-specific exposure to normal tissues. This finding is consistent with previous studies, indicating that liposomes can significantly improve therapeutic efficacy and reduce toxicity by enhancing drug delivery efficiency (such as clinical liposomal drugs like Doxil®) [22].

Second, *in vivo* experiments further verified the radioprotective potential of Ami liposomes. After TBI, the weight loss of mice in the liposome group was significantly lower than that in the free Ami group, and their behavioral scores were closer to those of the control group (Figs. 5(b) and 5(c)). Notably, this formulation not only protected the hematopoietic system (recovery of white blood cells, red blood cells, and platelet counts) and liver function (reduction of ALT/AST levels) but also

significantly alleviated radiation-induced lung and intestinal damage (Figs. 6 and 7). H&E staining showed that the lung tissue of mice in the liposome group had reduced inflammatory infiltration, and the colonic crypt structure was more intact, indicating its multi-organ protective properties. Additionally, *in vivo* metabolic experiments indicated that liposomes were mainly cleared through the kidneys without accumulation-related toxicity (Fig. 4(c)), providing a safety basis for its clinical translation.

The core mechanism of this study lies in revealing that Ami liposomes exert radioprotective effects by regulating the ferroptosis pathway. Ferroptosis, as an important mechanism of radiation damage, is characterized by lipid peroxidation, downregulation of GPX4 expression, and mitochondrial morphological abnormalities. The experiments showed that the liposome group effectively inhibited lipid peroxidation by upregulating GPX4 protein and mRNA expression (Figs. 8(a) and 8(b)), maintained mitochondrial membrane integrity (Fig. 8(c)), and thus blocked the ferroptosis process. This finding not only expanded the mechanism of action of Ami (traditionally focused on free radical scavenging) but also provided theoretical support for radioprotective strategies targeting ferroptosis.

To further enhance the clinical value of this formulation, our next steps will include the following: (1) active targeting modification: conjugating tumor-specific ligands (such as folic acid and transferrin) on the surface of liposomes to enhance drug enrichment in tumor tissues and reduce exposure to normal tissues; (2) combined treatment strategies: exploring the combined effects of Ami liposomes with other ferroptosis inhibitors (such as Ferrostatin-1) or radiosensitizers to achieve a 'protection-treatment' synergistic effect; (3) mechanism expansion: studying the influence of radiation microenvironments conditions (such as hypoxia and acidic pH) on the release kinetics of liposomal drugs to optimize their spatiotemporal controlled-release characteristics; (4) translational medicine validation: establishing preclinical large animal models of radiation-induced pneumonia or enteritis to evaluate the long-term efficacy and safety of the formulation, providing a basis for clinical trial design.

Conclusion

We have developed a novel nanomedicine by encapsulating Ami in liposome, which improves radiation protection and reduces the Ami toxicity, and this protection mechanism is closely linked to the regulation of ferroptosis a form of programmed cell death. This provides a new way to explore the development of radiation protection agents. At the same time, the application of these novel radiation protective agents in clinical RT has broad prospects.

Ethical Approvals

The authors are accountable for all aspects of the work in ensuring that questions related to the accuracy or integrity of any part of the work are appropriately investigated and resolved. The study was approved by the Ethics Committee of Zhongshan Hospital (No. 2023-246).

CRediT Author Statement

Y.K. Zhou, X. Ding, and **Y.X. Chen** conceived the project; **Y.N. Gao** carried out the synthesis of liposome amifostine and detected the radiation protection effect of amifostine liposomes *in vitro* and *in vivo*; **G.W. Guo** assisted in building mouse models of TBI; **Y. Zhuang** and **Y.X. Chen** performed flow cytometry, Western blot, tissue RNA extraction, and PCR; **F.Q. Zhang, J. He,** and **Y.N. Gao** wrote the manuscript.

Funding

This work was supported by the clinical research projects of Zhongshan Hospital, Fudan University (No. 2018ZSLC26), the youth fund of Zhongshan Hospital, Fudan University (No. 2024ZSQN12) and the Medical Guidance Program of the Science and Technology Commission of Shanghai Municipality (No. 22JC1402303).

Conflict of Interests

The authors declare that they have no known competing financial interests or personal relationships that could have appeared to influence the work reported in this paper.

Data Availability Statement

The data cannot be made publicly available upon publication because they are not available in a format that is sufficiently accessible or reusable by other researchers. The data that support the findings of this study are available upon reasonable request from the authors.

References

[1] S. Fan. Comparison of long-term outcomes of stereotactic body radiotherapy (SBRT) *via* helical tomotherapy for early-stage lung cancer with or without pathological proof. *Radiation Oncology,* 2023, 18: 49. https://doi.org/10.1186/s13014-023-02229-0

[2] Y.J. Xiong. Cathepsin L is involved in X-ray-induced invasion and migration of human glioma U251 cells. *Cellular Signalling,* 2017, 29: 181–191. https://doi.org/10.1016/j.cellsig.2016.10.012

[3] J.J. Lee. PTEN status switches cell fate between premature senescence and apoptosis in glioma exposed to ionizing radiation. *Cell Death and Differentiation,* 2010, 18: 666–677. https://doi.org/10.1038/cdd.2010.139

[4] J.P. Man. Biomaterials-mediated radiation-induced diseases treatment and radiation protection. *Journal of Controlled Release,* 2024, 370: 318–338. https://doi.org/10.1016/j.jconrel.2024.04.044

[5] J.L. Jiang. Advances and prospects in integrated nano-oncology. *Nano Biomedicine and Engineering,* 2024, 16: 152–187. https://doi.org/10.26599/NBE.2024.9290060

[6] L.X. Ye. Emphysema quantification on computed tomography and its value in predicting radiation pneumonitis in lung cancer treated by stereotactic body radiotherapy. *Journal of Radiation Research,* 2019, 60: 371–379. https://doi.org/10.1093/jrr/rrz007

[7] S. Shi. TMEM106A transcriptionally regulated by promoter methylation is involved in invasion and metastasis of hepatocellular carcinoma. *Acta Biochimica et Biophysica Sinica,* 2022, 54: 1008–1020. https://doi.org/10.3724/abbs.2022069

[8] D. Gao. Radiation-induced intestinal injury: Molecular mechanisms and therapeutic status. *DNA and Cell Biology,* 2024, 43: 537–548. https://doi.org/10.1089/dna.2024.0105

[9] X.Y. Li. GPX4 restricts ferroptosis of NKp46+ILC3s to control intestinal inflammation. *Cell Death and Disease,* 2024, 15: 687. https://doi.org/10.1038/s41419-024-07060-3

[10] X. Li. Ferroptosis inhibitor alleviates radiation-induced lung fibrosis (RILF) *via* down-regulation of TGF-β1. *Journal of Inflammation,* 2019, 16: 11. https://doi.org/10.1186/s12950-019-0216-0

[11] K. Jomova. Several lines of antioxidant defense against oxidative stress: Antioxidant enzymes, nanomaterials with multiple enzyme-mimicking activities, and low-molecular-weight antioxidants. *Archives of Toxicology,* 2024, 98: 1323–1367. https://doi.org/10.1007/s00204-024-03696-4

[12] S.P. Newman. Delivering drugs to the lungs: The history of repurposing in the treatment of respiratory diseases. *Advanced Drug Delivery Reviews,* 2018, 133: 5–18. https://doi.org/10.1016/j.addr.2018.04.010

[13] D.X. Zhang. Microalgae-based oral microcarriers for gut microbiota homeostasis and intestinal protection in cancer radiotherapy. *Nature Communications,* 2022, 13: 1413. https://doi.org/10.1038/s41467-022-28744-4

[14] Y. Wang. Copper in colorectal cancer: From copper-related mechanisms to clinical cancer therapies. *Clinical and Translational Medicine,* 2024, 14: e1724. https://doi.org/10.1002/ctm2.1724

[15] W. Zhang. GPX4, ferroptosis, and diseases. *Biomedicine and Pharmacotherapy,* 2024, 174: 116512. https://doi.org/10.1016/j.biopha.2024.116512

[16] J.M. Kim. Amifostine and melatonin prevent acute salivary gland dysfunction 10 days after radiation through anti-ferroptosis and anti-ferritinophagy effects. *International Journal of Molecular Sciences,* 2024, 25: 11613. https://doi.org/10.3390/ijms252111613

[17] C. Wang. Amifostine loaded lipid-calcium carbonate nanoparticles as an oral drug delivery system for radiation protection. *Biomedicine and Pharmacotherapy,* 2024, 177: 117029. https://doi.org/10.1016/j.biopha.2024.117029

[18] H.L. Zhou. Liposome-anchored mesenchymal stem cells for radiation pneumonia/fibrosis treatment. *Biomaterials,* 2023, 300: 122202. https://doi.org/10.1016/j.biomaterials.2023.122202

[19] S. Shah, V. Dhawan, R. Holm, et al. Liposomes: Advancements and innovation in the manufacturing process. *Advanced Drug Delivery Reviews,* 2020, 154–155: 102–122. https://doi.org/10.1016/j.addr.2020.07.002

[20] J. Li, Y. Wang, W. Shen, et al. Mitochondria-modulating liposomes reverse radio-resistance for colorectal cancer. *Advanced Science,* 2024, 11(18): 2400845. https://doi.org/10.1002/advs.202400845

[21] D. Guimarães, A. Cavaco-Paulo, E. Nogueira, Design of liposomes as drug delivery system for therapeutic applications. *International Journal of Pharmaceutics,* 2021, 601: 120571. https://doi.org/10.1016/j.ijpharm.2021.120571

[22] Y. Barenholz. Doxil®—the first FDA-approved nano-drug: Lessons learned. *Journal of Controlled Release,* 2012, 160: 117–134. https://doi.org/10.1016/j.jconrel.2012.03.020